Drug Delivery and Translational Research (2019) 9:273–283
https://doi.org/10.1007/s13346-018-0591-8

ORIGINAL ARTICLE

Synthesis and characterization of a new cyclodextrin derivative with improved properties to design oral dosage forms

Agustina García[1,2] · Josefina Priotti[1] · Ana Victoria Codina[3,4] · María Delia Vasconi[3,5] · Ariel D. Quiroga[6] · Lucila I. Hinrichsen[3,4] · Dario Leonardi[1,2,7] · María Celina Lamas[1,2,7]

Published online: 28 September 2018

Abstract

This work aimed to synthesize a novel β-cyclodextrin derivative, itaconyl-β-cyclodextrin to evaluate whether albendazole inclusion complexes with the new β-cyclodextrin derivative-improved albendazole dissolution efficiency and its anthelminthic activity. The new derivative was thoroughly evaluated and characterized, and an average degree of substitution of 1.4 per cyclodextrin molecule was observed. Albendazole:itaconyl-β-cyclodextrin complexes were prepared by spray drying procedures and investigated using phase solubility diagrams, dissolution efficiency, X-ray diffraction, differential scanning calorimetry, Fourier transform infrared, scanning electronic microscopy, mass spectrometry, and nuclear magnetic resonance spectroscopy. Phase solubility diagrams and mass spectrometry studies showed that the inclusion complex was formed in an equimolar ratio. Stability constant values were 602 M^{-1} in water, and 149 M^{-1} in HCl 0.1 N. Nuclear magnetic resonance experiments of the inclusion complex showed correlation signals between the aromatic and propyl protons of albendazole and the itaconyl-β-cyclodextrin inner protons. The studies indicated solid structure changes of albendazole included in itaconyl-β-cyclodextrin. The maximum drug release was reached at 15 min, and the inclusion complex solubility was 88-fold higher than that of the pure drug. The in vitro anthelmintic activity assay showed that the complex was significantly more effective than pure albendazole.

Keywords Cyclodextrins · Synthesis · Poorly water-soluble drug · Albendazole · Physicochemical characterization

Introduction

Strategies for enhancing dissolution of poorly water-soluble drugs can be classified mainly into two groups: chemical and physical. One of the chemical strategies involves the modification of the molecule by incorporating functional groups to increase drug hydrophilicity or to induce ionization in the gastrointestinal fluids [1]. Physical strategies include to modify drug solid state; particle size reduction; optimize the solubilization process employing co-solvents and surfactants. These all physical strategies are relatively simple procedures to achieve an improvement in biopharmaceutical properties. Special attention needs to be paid to metastable polymorphs, salts, co-crystals, and amorphous forms that tend to

✉ Dario Leonardi
leonardi@iquir-conicet.gov.ar

✉ María Celina Lamas
mlamas@fbioyf.unr.edu.ar

[1] IQUIR-CONICET, Suipacha 570, 2000 Rosario, Argentina

[2] Departamento de Farmacia, Facultad de Ciencias Bioquímicas y Farmacéuticas, Universidad Nacional de Rosario, Suipacha 570, 2000 Rosario, Argentina

[3] Instituto de Genética Experimental, Facultad de Ciencias Médicas, Universidad Nacional de Rosario, Santa Fe 3100, 2000 Rosario, Argentina

[4] CIC-UNR, Universidad Nacional de Rosario, Maipú 1065, 2000 Rosario, Argentina

[5] Área Parasitología, Facultad de Ciencias Bioquímicas y Farmacéuticas, Universidad Nacional de Rosario, Suipacha 570, 2000 Rosario, Argentina

[6] Instituto de Fisiología Experimental (IFISE-CONICET), Suipacha 570, 2000 Rosario, Argentina

[7] Facultad de Ciencias Bioquímicas y Farmacéuticas, Universidad Nacional de Rosario, Suipacha 531, 2000 Rosario, Argentina

recrystallize into their most stable form. The reduction of particle size presents the risk of agglomeration and crystal growth. Dosage forms using surfactants and lipids are highly versatile, but they require extensive characterizations and can be related to the following risks: toxicity of the excipients, drug precipitation, and modification of the pharmacokinetic profile and biodistribution [2].

Another significant physical strategy to improve the solubility of poorly soluble compounds is the preparation of inclusion complexes with cyclodextrins (CDs). CDs have been studied for over 100 years, yet they are still considered novel pharmaceutical excipients [3]. They have been gaining interest in the past years, alongside the rise of a variety of substituted CDs. Besides an enhanced solubility, drug inclusion complexes can lead to improve drug availability, and drug stability by preventing degradation. CDs are a family of cyclic oligosaccharides that possess biological properties similar to those of their linear counterparts [3, 4]. The three most widely used CDs (α, β, and γ) are crystalline, homogeneous, and non-hygroscopic excipients [5]. The fact that oligomeric CD molecules are formed by six to eight glucopyranose units bound via α-1,4 glycosidic linkages provides this group of supramolecular compounds with remarkable advantages. The CD molecule can be conceived as a truncated cone with a hydrophilic exterior. The cone inner walls are formed by the hydrophobic carbon backbones of the glucopyranose units, generating a hydrophobic interior. This particular structure supports the use of CDs as solubilizers of poorly water-soluble chemicals [6–8].

Nevertheless, β-CD shows considerably low solubility in water and this issue can be overcome by chemical modification obtaining randomly substituted heterogeneous products, non crystallizable, useful for the pharmaceutical industry [4]. CD crystallinity is thought to be due to relatively strong intermolecular hydrogen bonding in the crystalline state. Substitution of any of the hydrogen bonds forming hydroxyl groups results in notable improvement in its aqueous solubility [9, 10]. CD derivatives of pharmaceutical interest include the hydroxypropyl derivatives of β and γ-CD, the randomly methylated-β-CD, sulfobutylether-β-CD, citrate-β-CD, succinyl-β-CD, and the branched CDs such as glucosyl-β-CD [7, 9–11].

Since CDs can form water-soluble inclusion complexes with many poorly soluble lipophilic drugs, they are used to enhance the drug aqueous solubility and to improve its bioavailability after oral administration [12, 13]. The formation of complexes with CDs is one of the several strategies employed to increase solubility, dissolution rate and oral bioavailability of such poorly water-soluble drugs [9, 11, 14, 15].

Albendazole (ABZ), a benzimidazole carbamate, is an anthelmintic compound showing larvicide, ovicide, and vermicide activity. It is widely used in the treatment of trichinellosis, a parasitic disease caused by the helminth *Trichinella* spp. [11, 13]. Its effectiveness is limited by its poor water solubility (1 μg/mL at 25 °C) and the consequent low bioavailability, producing in some cases an unpredictable therapeutic response.

The synthesis of a novel CD derivative, itaconyl-β-CD (I-β-CD), to optimize the oral administration of poorly soluble compounds, mainly those with basic characteristics such as ABZ, is an attractive matter to improve the current anthelmintic therapeutic alternatives. Indeed, inclusion complexes formation is markedly improved by the interaction when the CD and the drug have opposite charges [12, 16].

The characterization of I-β-CD and its inclusion complexes is fundamental to understand the host-guest molecule interaction. Different experiments of nuclear magnetic resonance (NMR) spectroscopy and mass spectrometry have been used to characterize them [9, 10].

Thus, this paper describes a simple and interesting method to synthesize a novel CD derivative and its application on ABZ complexation, as well as the complete physicochemical characterization of the derivative and its complexes using different techniques. Additionally, the in vitro anthelminthic activity of the formulations was evaluated on *Trichinella spiralis* (*T. spiralis*) adult parasites.

Materials and methods

Materials

ABZ, $NaH_2PO_2.H_2O$, and itaconic acid (IA) were purchased from Sigma-Aldrich (Chemie GmbH, Steinheim, Germany), and β-CD was donated by Roquette (France). Hydroxypropyl-β-CD (HP-β-CD) and methyl-β-CD (M-β-CD) were purchased from Sigma-Aldrich (Chemie GmbH, Steinheim, Germany). Absolute ethanol was obtained from Laboratorio Cicarelli (Argentina). RPMI 1640 medium was purchased from Gibco Laboratories (USA), fetal bovine serum from Natocor (Argentina), and gentamicin from Klonal (Argentina). All other chemicals used were of analytical reagent grade.

Methods

Synthesis of I-β-CD

The synthesis of I-β-CD was carried out by reflux heating. IA (8.12 mmol, 1.056 g) was dissolved in distilled water (0.8 mL), then $NaH_2PO_2.H_2O$ (0.58 mmol, 62.5 mg) and β-CD (1.16 mmol, 1.316 g) were added. Molar ratio between β-CD and IA was 1:7. The mixture was heated at 120 °C for 5 h. After that, 20 mL of absolute ethanol were added to separate the desired product by precipitation. The precipitate was filtered and washed until the pH of the supernatant was neutral, which indicates that there was no free IA remaining. Finally, the reaction product (I-β-CD) was dried 24 h at 60 °C [17].

Characterization of I-β-CD

The yield of the β-CD derivative was calculated by the relationship between the moles of I-β-CD and the moles of starting β-CD.

Solution NMR spectra, 1D ^{1}H, ^{13}C and ^{1}H-^{1}H TOCSY, 2D ^{1}H-^{1}H COSY, ^{1}H-^{13}C HSQC, and ^{1}H-^{13}C HMBC, were recorded on a Bruker Avance 300 MHz NMR spectrometer (Karlsruhe, Germany). Samples of I-β-CD were prepared in D_2O (24 mM) (δ 4.7 ppm).

The mass spectrum was performed on a Bruker micrOTOF-Q II mass spectrometer (Bruker-Daltonics, Bremen, Germany). The analysis conditions were as follows: ESI negative mode, scan 200–2000 m/z, nebulizer pressure 0.4 bar, temperature 180 °C, drying gas flow rate 4.0 L/min, capillary voltage 4500 V, and collision energy 35 eV.

I-β-CD molecular weight and degree of substitution (DS) were calculated from NMR and mass spectrometry studies [9, 10].

DS was determined from ^{1}H NMR spectrum by using Eq. 1:

$$\mathrm{DS} = \frac{\mathrm{A_{H-b^{'}}} + \mathrm{A_{H-b^{*}}}}{2\ \mathrm{x}\ (\mathrm{A_{H-1}})} \quad (1)$$

where $A_{H\text{-}1}$ is the H-1 proton peak area, while $A_{H\text{-}b^{*}}$ and $A_{\mathbf{H\text{-}b}}$, correspond to the vinyl proton peak areas.

Besides, DS was calculated according to Eq. 2, assuming that the spectrometer has the same sensitivity for CDs with different DS.

$$\mathrm{DS} = \frac{\sum_i i \times \mathrm{DS}_i}{\sum_i I_i} \quad (2)$$

where I_i and DS_i denote the intensity and the DS of peak ith, respectively.

Preparation and characterization of ABZ:I-β-CD systems

Phase solubility diagrams The phase solubility assay was carried out as follows. An excess of ABZ (~ 25 mg) was added to vials containing 5 mL of increasing concentration solutions, from 0 to 50 mM (0, 65.0, 129.9, 194.9, 259.8, and 324.8 mg), of I-β-CD in 0.1 N HCl (pH 1.2) or bidistilled water. Solutions were stirred (200 rpm) for 72 h at 25 °C. Afterward, solutions were filtered through a 0.45-μm pore size syringe filter and ABZ concentration was determined by UV-spectrophotometry at 292 nm. The complex formation constant (K_f) was calculated from the slope (S) and intercept (S_o) of the phase solubility diagram, according to Eq. 3 reported by Higuchi and Connors: [5, 18].

$$K_f = \mathrm{S}/\mathrm{S_o}(1-\mathrm{S}) \quad (3)$$

The same procedure was repeated employing β-CD, HP-β-CD, and M-β-CD to compare the K_f values.

Preparation of ABZ:I-β-CD systems The inclusion complex was prepared in a molar ratio of 1:1 (ABZ:I-β-CD). ABZ (0.565 mmol, 150 mg) was solubilized in 10 mL of glacial acetic acid and I-β-CD (0.565 mmol, 734.4 mg) in 20 mL of water. Both solutions were mixed under stirring and immediately dried in a Mini Büchi Spray Dryer B-290 (Flawil, Switzerland) at 130 °C with a feed rate of 5 mL/min [19, 20].

In addition, a physical mixture of ABZ and I-β-CD was prepared for comparison, by mixing both compounds in a mortar for 10 min.

Yield and ABZ content of spray dried complex The complex yield was calculated according to the following equation:

$$\mathrm{Yield}\ (\%) = \frac{\mathrm{W_{product}}}{\mathrm{W_{ABZ}} + \mathrm{W_{I-\beta-CD}}} \times 100 \quad (4)$$

where $W_{product}$ is the weight of the product obtained after spray drying, W_{ABZ} and $W_{I\text{-}\beta\text{-}CD}$ are the weights of raw materials ABZ and I-β-CD, respectively.

The determination of the ABZ content was carried out by UV spectrophotometry. Briefly, a sample of 20.0-mg complex was dissolved in a 100-mL volumetric flask with 0.1 M HCl.

ABZ concentration solution was determined at 292 nm and the ABZ content of spray dried complex was calculated as percentage (*w*/*w*).

Characterization of the ABZ:I-β-CD systems The morphology of ABZ, I-β-CD, ABZ:I-β-CD physical mixture (PM), and inclusion complex powders by spray drying (SD) was studied through images by scanning electronic microscopy (SEM) on a Leitz AMR 1600 T, with an accelerating potential of 20 kV. Samples were previously distributed on an aluminum support and gold sputter-coated to make them conductive.

Differential scanning calorimetry (DSC) measurements were conducted on a Shimadzu TA-60 calorimeter (Kyoto, Japan). Each sample was placed in a crimped aluminum pan and scanned from 25 to 300 °C at a rate of 5 °C/min, under a nitrogen flow of 30 mL/min. Calibration was performed with indium and zinc as standards [20, 21].

An automated X'Pert Philips 5000 diffractometer (Eindhoven, The Netherlands) was used for X-Ray diffraction (XRD) analysis, in reflexion mode at room temperature. Diffraction data were obtained using Cu-Kα radiation (k = 1.54056 Å), applying 40 kV and 20 mA, with a step size of $2\theta = 0.02°$ [22].

Fourier transform infrared (FT-IR) spectra of the samples were recorded using KBr disk method on an FT-IR-Prestige-21 Shimadzu spectrometer (Tokyo, Japan). Scanning range was 450–3900 cm^{-1} with a resolution of 1 cm^{-1}.

^{1}H, ^{13}C, ^{1}H-^{1}H COSY, ^{1}H-^{13}C HSQC, ^{1}H-^{13}C HMBC, and ROESY experiments were carried out on a Bruker Avance 300 MHz NMR spectrometer (Karlsruhe, Germany). ABZ:I-β-CD complex (10 mg) was dissolved in 0.1 N DCl. ROESY spectra were acquired with 32 scans, an acquisition time of 0.222 s and a relaxation delay of 2 s.

The stoichiometry of the complex was confirmed by mass spectrometry on a micrOTOF-Q II spectrometer (Bruker-Daltonics, Germany). ABZ:I-β-CD complex (1 mg) was dissolved in formic acid (1 mL, 0.4% *v*/*v*), and was diluted 1/100 with a methanol:water mixture (50:50). The analysis conditions were as follows: ESI method, negative mode, collision energy − 10 eV, nebulizer 0.4 bar, temperature 180 °C, flow rate of the drying gas 4.0 L/min, and m/z range 50–3000.

Apparent solubility Solubility assays were conducted by adding an excess amount of the PM or the inclusion complex prepared by SD in vials with 10 mL of distilled water. The vials were sealed and stirred for 72 h at 200 rpm. Afterward, solutions were filtered using 0.45-μm syringe filters and ABZ concentrations were obtained by UV-spectrophotometry at 292 nm. All determinations were done in triplicate. Additionally, apparent solubility assays of ABZ:β-CDs systems were carried out to make a comparison with commercially available CDs (β-CD, HP-β-CD, and M-β-CD).

Dissolution studies The dissolution studies were performed using the paddle method (USP apparatus II Hanson Research SR8 Plus, Chatsworth, USA), according to the USP XXXII [23]. Samples containing 100 mg of ABZ were added into dissolution vessels with 900 mL of HCl 0.1 N at 37.0 ± 0.1 °C; the temperature was maintained within that range during the whole process. Solution aliquots (5 mL) were collected at different times to determine drug release spectrophotometrically [24].

Additionally, dissolution efficiency (DE) of ABZ powder, PM, and inclusion complex (SD) was calculated applying Eq. 5.

$$\mathrm{DE}\ (\%) = \frac{\int_0^t y \times \mathrm{dt}}{\mathrm{y}_{100} \times \mathrm{t}} \times 100 \tag{5}$$

where $\int_0^t y \times dt$ is the area under the dissolution curve in an interval of time t, and $y_{100} \times t$ is the rectangle area considering 100% dissolution at the same interval.

Dissolution studies of complexes with commercial CDs (β-CD, HP-β-CD, and M-β-CD) obtained by PM and SD were performed to compare them with the new derivative.

In vitro evaluation of the anthelmintic activity of the ABZ-I-β-CD systems on Trichinella spiralis adult parasites *T. spiralis* female worms were obtained from a donor mouse during the intestinal phase of the infection, on day 6 post-infection, as already described [25, 26].

ABZ, I-β-CD, ABZ:I-β-CD (PM), and ABZ:I-β-CD (SD) stock solutions were prepared in DMSO and were added to RPMI 1640 medium supplemented with 250 μg/mL of gentamicin, to obtain working solutions with a final concentration of 500 μg ABZ/mL. Each working solution was prepared, stirred for 24 h at 150 rpm and 25 °C and filtered through a 0.22-μm sterile cellulose acetate filter, before use.

The in vitro assay was done under sterile conditions. *T. spiralis* female worms were incubated overnight in the RPMI 1640 medium supplemented with gentamicin (250 μg/mL) and fetal bovine serum (10% *v*/*v*), at 37 °C, in a 5% CO_2 atmosphere, before being used. The antiparasitic activity assay was done in a 24-well plate, placing 1.8 mL of the working solutions, 200 μL fetal bovine serum and 10 to 12 females in each well. The ABZ solution was used as a positive control and the culture medium with the solvent employed as a negative control. Plates were incubated in a humid 5% CO_2 atmosphere at 37 °C for 48 h and were observed under an inverted microscope at 2, 4, 6, 24, 30, and 48 h to count the dead worms. Parasites viability was estimated analyzing their motility and morphology, and they were classified into two categories: (0) dead; (1) alive, with normal morphology and varying degrees of motility [27]. The ABZ solution was used as the positive control and the culture medium with DMSO as the negative control. The assay was made in triplicate. Data were corrected by the negative control median at each time point. The efficacy of the different antiparasitic treatments was assessed by analyzing parasite survival with the Kaplan-Meier survival curve, which defines the probability of surviving in a given length of time while considering time in many small intervals; each time point represents the median percentage of live parasites.

T. spiralis female fertility was also evaluated by the number of newborn larvae (NL) per well at each time point. Fertility was scored as follows: (0) no NL in the well, (+) 1 to 30 NL, and (++) more than 30 NL.

Statistical analysis

Apparent solubility values and DE values between ABZ:β-CDs systems were analyzed. One-way ANOVA tests were used followed by Tukey's multiple comparison tests. As regards in vitro experiments, survival curves were calculated with the product limit method of Kaplan and Meier. Comparison of the survival curves was done with the log-rank test.

GraphPad Prism 7.00 (GraphPad Software, Inc., San Diego, CA) was used to calculate all statistics. P values < 0.05 were considered significant.

Results and discussion

Characterization of I-β-CD

The I-β-CD derivative was obtained with a yield of 71%. A complete characterization by NMR analysis was carried out to determine the I-β-CD derivative substitution pattern. The assignment of the ^{1}H and ^{13}C peaks are exhibited in the horizontal and vertical projections of the HSQC spectrum, respectively (Fig. 1). ^{1}H-^{13}C HSQC spectrum showed a ^{1}H signal at δ 3.34 ppm that was correlated with a ^{13}C signal at δ 37.90 ppm; these signals correspond to methylene groups of the itaconyl substituent (a and a', Fig. 1).

Two peaks were observed in the ^{1}H NMR spectrum at 4.45 and 4.18 ppm which presented cross-peaks with the ^{13}C peak at 64.38 ppm on the multiplicity-edited HSQC spectrum. These signals correspond to the substituted nuclei at position 6 (X6sub). A downfield shift in these signals position with respect to those produced by the non-substituted homologous nuclei resulted from the deshielding of the nucleus by the substituent. The presence of signals corresponding to unsubstituted nuclei at position 6 indicates a partial substitution of the I-β-CD. The average DS could be quantified from the proton peak areas. As shown in Fig. 1, H-b' and H-b* did not overlap, thus DS could be determined by comparing the sum of these two peaks (which integrated two protons) to the peak area of H1 (which integrated one proton). DS obtained from ^{1}H NMR was 1.40 per CD molecule. The DS analysis was carried out over three batches and the relative standard deviation (variation coefficient) obtained for this parameter was 4.2%, indicating a high reproducibility in the synthesis of this derivative.

The I-β-CD mass spectrum (Fig. 2), performed in negative ionization mode, shows the ions with m/z ratios of 1245.4, 1357.4, and 1469.4, which correspond to I-β-CD molecules with one, two, or three substituents, respectively. These ions had a clearly asymmetric distribution; the peak with greater intensity was due to the derivative with one substituent. The DS calculated by Eq. 2 was 1.52, which was consistent with that obtained by NMR.

Characterization of the ABZ:I-β-CD systems

Yield, ABZ content, and solubility studies

The spray drying technique allowed to obtain the ABZ:I-β-CD inclusion complex with a yield of 80% and an ABZ content of 17.2% (*w*/*w*). This value was in agreement with the molar ratios between both compounds (1:1) and their molecular weights.

The phase solubility diagrams of ABZ inclusion complex (I-β-CD) in water and HCl (Fig. 3a) showed a linear relationship between ABZ and the CD derivative. Similarly, the phase solubility diagrams carried out in water, (ABZ:β-CD, ABZ:HP-β-CD, ABZ:M-β-CD, and ABZ:I-β-CD) showed a linear relationship between ABZ and the CDs, fitting an A_L-type system (Fig. 3b). This type of curves indicates the formation of soluble 1 : 1 type inclusion complex.

The K_f value obtained for the inclusion complex between ABZ and I-β-CD was 602 M^{-1}, denoting a relatively more stable complex in comparison with those obtained with traditional CDs (β-CD, 74 M^{-1}; HP-β-CD, 313 M^{-1}; and M-β-CD, 337 M^{-1}). This greater stability of the ABZ:I-β-CD inclusion complex could be explained by interaction charges

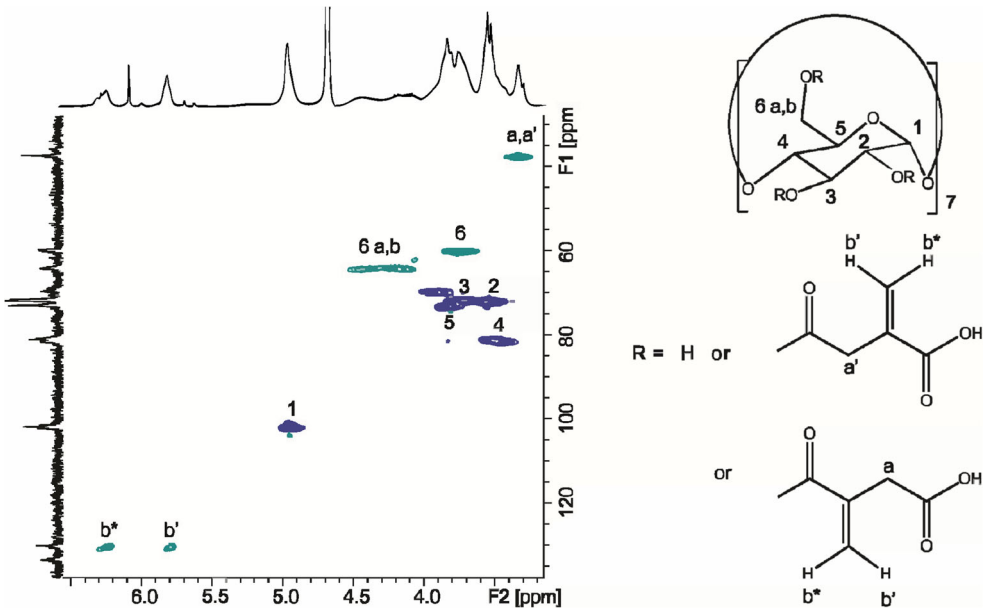

Fig. 1 I-β-CD HSQC spectrum

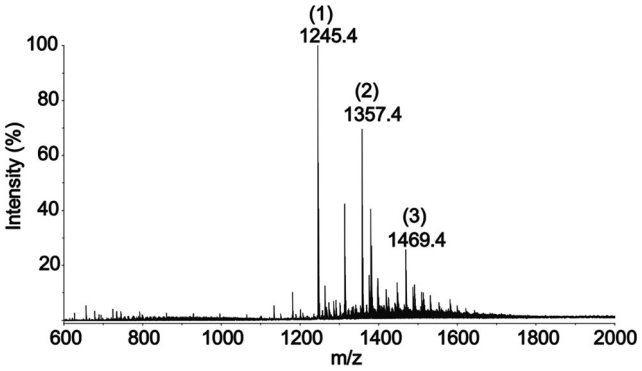

Fig. 2 I-β-CD mass spectrum

between the carboxylic groups of the derivative and the amino groups of ABZ.

The K_f values for ABZ:I-β-CD system were 602 M^{-1} in water and 149 M^{-1} in HCl 0.1 N. As expected, ABZ intrinsic solubility (S_0) was higher at acidic pH. However, this improvement of solubility obtained at acidic pH reduced the stability of the complex. A lower K_f value could be attributed to the lower affinity of the positively charged ABZ for the hydrophobic I-β-CD cavity. After administering the complex orally, ABZ would be easily released from the I-β-CD cavity into the stomach, facilitating its absorption.

SEM micrographs

Figure 4 shows micrographs of ABZ, I-β-CD, and ABZ:I-β-CD systems obtained by SD and PM. ABZ particles (Fig. 4a) had an irregular form and were larger than 10 μm in diameter. I-β-CD solid particles presented spherical shape and smooth and variable surface. The PM system micrograph allows to clearly visualize ABZ and I-β-CD maintaining their original structure and size. On the contrary, the finding of predominantly spherical particles (Fig. 4d) suggests the formation of a new structure in the solid state between ABZ and I-β-CD in the SD system [28].

XRD diffractograms

The ABZ XRD diffractogram (Fig. 5a) showed intense and sharp peaks at 2θ 11.51; 17.85; 22.09, and 24.54, indicating that this compound was in a crystalline state. Contrariwise, the broad peaks observed in the I-β-CD diffractogram signified that it was in an amorphous state. The XRD pattern of the ABZ:I-β-CD system obtained by PM showed the characteristic peaks of ABZ (2θ 11.51, 17.85, 22.09, and 24.54) as well as those of I-β-CD. Conversely, the diffractogram from the ABZ:I-β-CD system obtained by SD only showed the signals at 2θ 17.85 and 24.54 corresponding to ABZ, but with a lower intensity than those of the diffractogram from the system obtained by PM. These results suggest a change in the solid structure of the inclusion complex in comparison with the starting materials [29, 30].

DSC thermograms

ABZ, I-β-CD, and both ABZ:I-β-CD systems DSC thermograms (Fig. 6) were performed to evaluate whether changes in the ABZ melting peak occurred when combined with I-β-CD and whether the preparation method influenced those changes. The characteristic melting peak of ABZ appeared at 196.84 °C. This peak was also observed in the PM thermogram and, though present, it was less intense in the thermogram of the system prepared by SD. This could be due to a modification in the crystallinity of the drug loaded in the last system. These results agreed with those obtained by XRD analysis [28].

FT-IR analysis

Figure 7 shows the results of the FT-IR analysis. ABZ FT-IR spectrum presented the characteristic transmittance bands at 3332 cm^{-1} (N–H stretching vibration), 2954 and 2927 cm^{-1} (CH_3/CH_2 groups), 2661 cm^{-1} (vibrations of the C-H links), 1712 cm^{-1} (amide band), 1632 cm^{-1} (stretching vibration of the aromatic rings), 1589 cm^{-1} (stretching vibration of

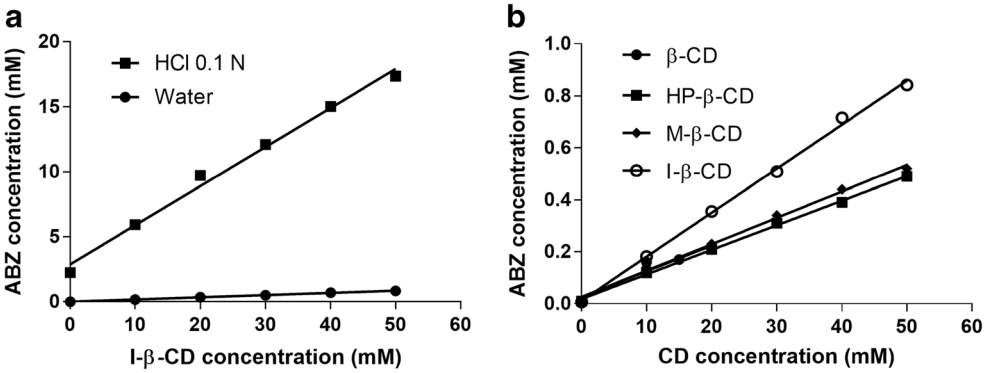

Fig. 3 Phase solubility diagrams. Concentration of ABZ against increasing concentrations of I-β-CD, in water or in HCl 0.1 N (**a**). Comparison of I-β-CD and commercial CDs in water (**b**)

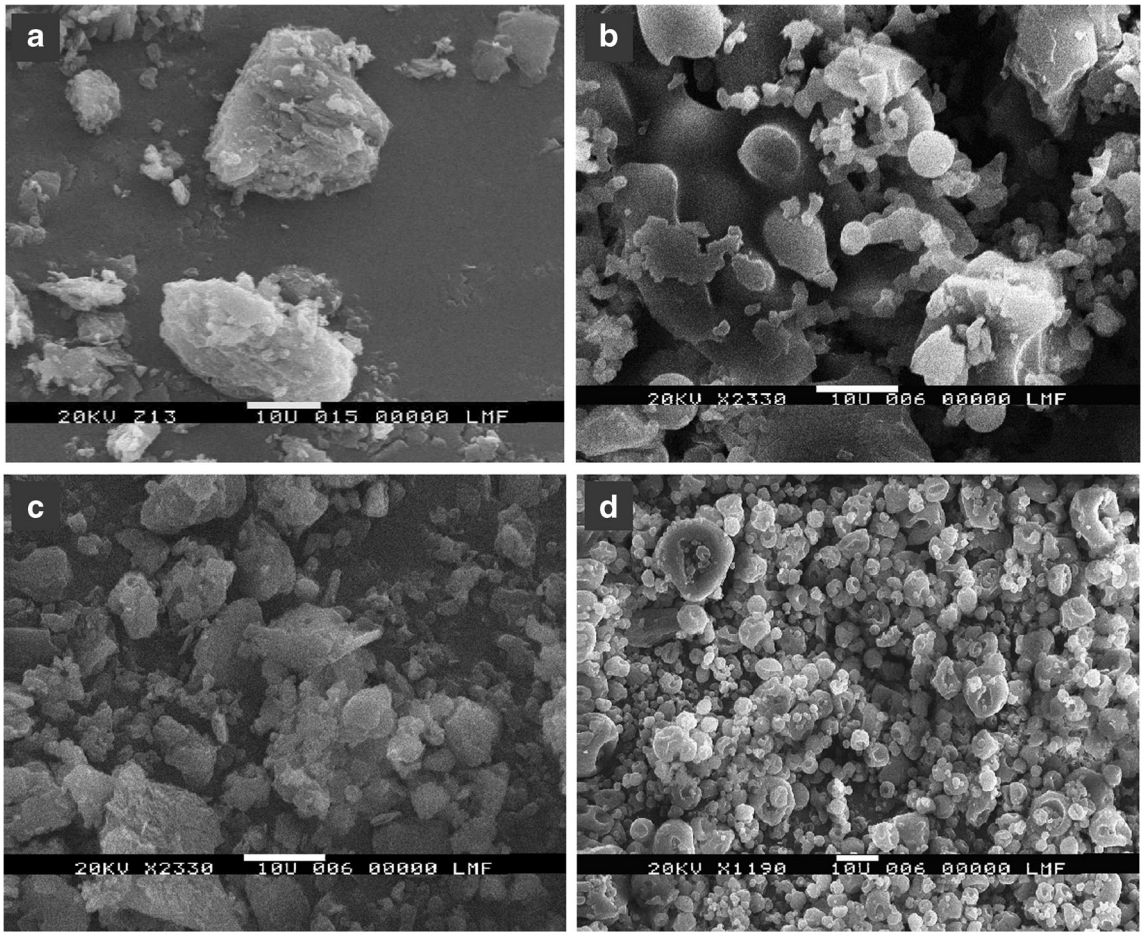

Fig. 4 SEM micrographs. ABZ (**a**), I-β-CD (**b**), ABZ:I-β-CD (PM) (**c**), and ABZ:I-β-CD (SD) (**d**)

aromatic C–N bonds), and 1523 cm^{-1} (amide band). I-β-CD FT-IR spectrum showed wide bands with a transmittance peak at 3385 cm^{-1} corresponding to the symmetric and asymmetric stretching vibration of the −OH groups, and another band at 2929 cm^{-1} related to the stretching vibration of the C–H bonds. The transmittance peaks at 1157 cm^{-1} and 1028 cm^{-1} were due to the asymmetric and symmetric stretching vibration corresponding to the C–O–C bonds. On the other hand, the peak at 1734 cm^{-1} marked the ester bond formed between the carboxylic groups of IA and the hydroxyls of β-CD.

The FT-IR spectra from the systems showed absorption bands corresponding to both I-β-CD and ABZ. There were no remarkable differences between the two spectra, except for the absorption bands at 3332 cm^{-1} (found superimposed with that originated by the OH groups of the CD) and 2954 cm^{-1} (corresponding to ABZ), observed only in the spectrum of the PM. These results indicated structural differences produced by the SD process in the ABZ:I-β-CD system. [31, 32]

ROESY NMR experiments

ROESY NMR experiments are relevant to determine inter and intramolecular interactions. Closely located protons can produce a nuclear Overhauser effect (NOE) cross-correlation in ROESY; the presence of NOE cross-peaks indicates spatial contacts within 0.4 nm between two species.

ABZ and I-β-CD proton labels, and the ROESY spectrum from the ABZ:I-β-CD system obtained by SD are shown in Fig. 8. In this spectrum, the I-β-CD internal protons (H3, H5, H6) presented cross-peaks with the aromatic protons of ABZ (e:

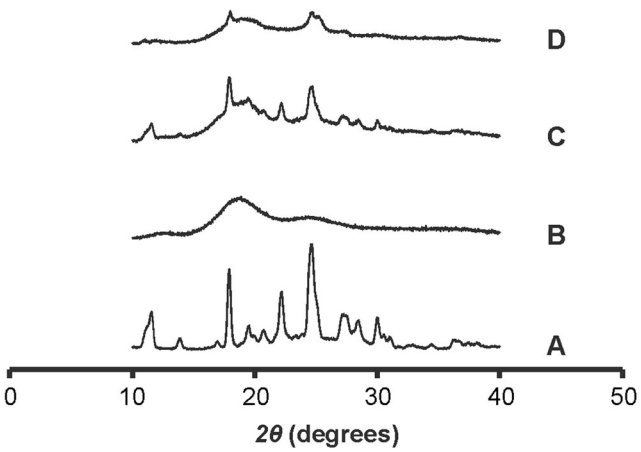

Fig. 5 XRD diffractograms. ABZ (**a**), I-β-CD (**b**), ABZ:I-β-CD (PM) (**c**), and ABZ:I-β-CD (SD) (**d**)

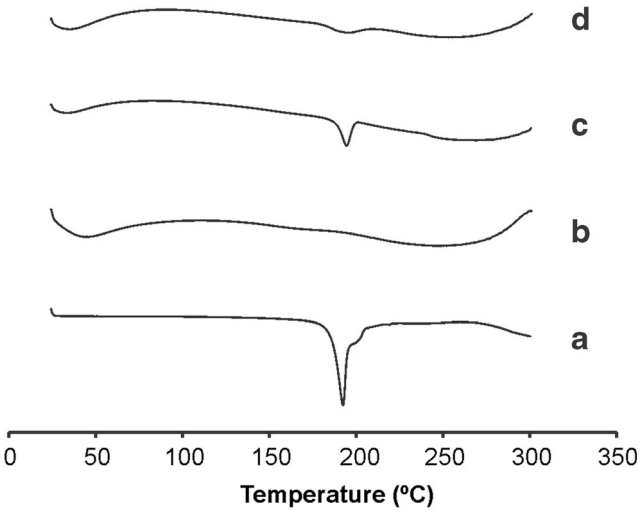

Fig. 6 DSC thermograms. ABZ (**a**), I-β-CD (**b**), ABZ:I-β-CD (PM) (**c**), and ABZ:I-β-CD (SD) (**d**)

δ = 7.24 ppm, f: δ = 7.37 ppm, and g: δ = 7.40 ppm). These protons also showed signals of correlation with protons a, b, and c of ABZ, the correlation with protons b being weak (a: δ = 0.80 ppm, b: δ = 1.40 ppm and c: δ = 2.79 ppm, Fig. 7).

The ROESY spectrum allowed us to conclude that both the aromatic ring and the tail of ABZ are inside the CD derivative.

The relative abundances and stoichiometries of the inclusion complex ABZ:I-β-CD prepared by SD were determined by mass spectrometry. The spectrum showed a molecular ion with an m/z ratio of 1512.5, corresponding to equimolar complexes between molecules of ABZ and I-β-CD with a single substituent.

Also, no signals with an m/z ratio related to complexes formed with I-β-CD molecules with more than one substituent or in a stoichiometric ratio other than 1:1 were observed. This last result agrees with that obtained from the phase solubility diagrams made for ABZ in the presence of I-β-CD [33–37].

Apparent solubility and dissolution studies

Apparent solubility values of ABZ:β-CDs systems are shown in Table 1. ABZ:β-CDs systems obtained by SD presented higher solubility values than their respective PMs in all cases. It should be noted that apparent solubility of ABZ:I-β-CD systems (PM and SD) was at least 5-fold higher than the other systems and showed statistically significant differences.

Figure 9 presents the dissolution profiles of the ABZ:I-β-CD systems obtained by SD and PM as well as those of

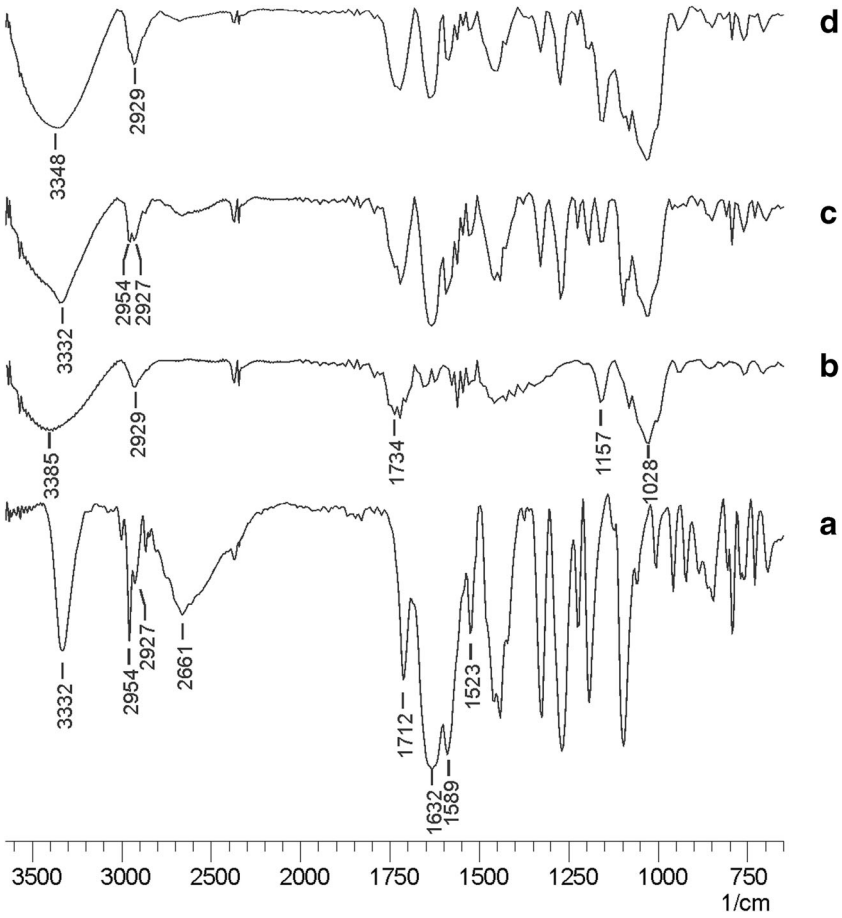

Fig. 7 FT-IR spectrum. ABZ (**a**), I-β-CD (**b**), ABZ:I-β-CD (PM) (**c**), and ABZ:I-β-CD (SD) (**d**)

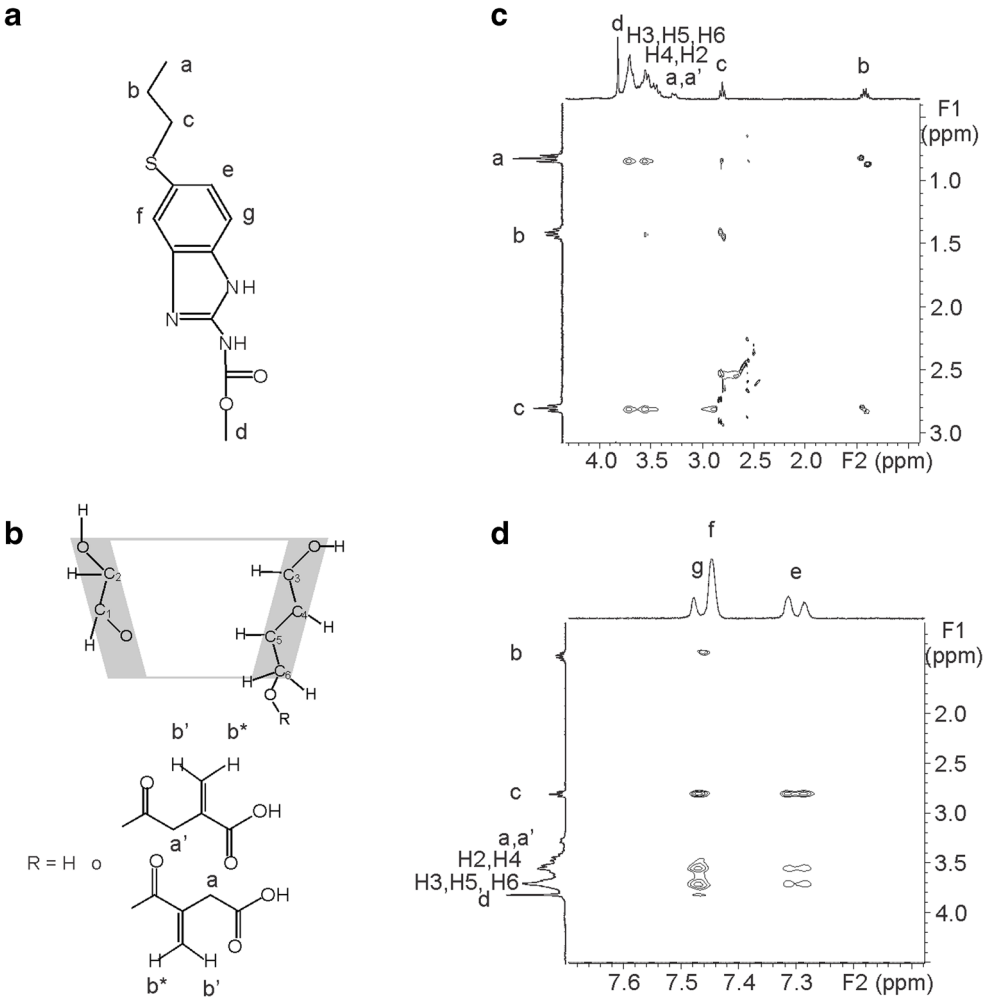

Fig. 8 ROESY spectrum. ABZ proton labelling (**a**), I-β-CD (**b**), plot of the 2D ROESY spectrum of ABZ in the presence of I-β-CD (**c**, **d**)

similar systems formulated with ABZ and β-CD to evaluate the efficiency of I-β-CD as a carrier. Analyzing the dissolution profile of the ABZ:I-β-CD system obtained by SD, the maximum percentage of dissolved ABZ was reached 15 min after the start of the test.

As can be seen in Table 1, dissolution parameters for ABZ:I-β-CD (SD) were higher and statistically significant than those percentages obtained for the analog systems prepared with commercial CD derivatives, except for the system formulated with M-β-CD.

Table 1 Values of apparent solubility at 25 °C and dissolution parameters (Q_{30}, Q_{60}, and DE) of ABZ:CDs systems obtained by PM and SD. ($n = 3$, ± SD)

System	Solubility (mg/mL)	Q_{30} (%)	Q_{60} (%)	DE (%)
ABZ:β-CD PM	0.013 ± 0.002	7.7 ± 0.1	12.6 ± 0.2	16.9
ABZ:β-CD SD	0.024 ± 0.001	34.5 ± 1.9	46.6 ± 1.4	55.4
ABZ:M-β-CD PM	0.016 ± 0.001	62.9 ± 1.1	68.3 ± 1.4	70.3
ABZ:M-β-CD SD	0.069 ± 0.002	99.0 ± 2.1	94.8 ± 1.3	92.8
ABZ:HP-β-CD PM	0.011 ± 0.004	22.5 ± 0.9	31.3 ± 1.1	36.6
ABZ:HP-β-CD SD	0.048 ± 0.001	54.8 ± 2.0	65.6 ± 1.2	69.8
ABZ:I-β-CD PM	0.088 ± 0.003	13.0 ± 0.1	18.9 ± 0.8	23.4
ABZ:I-β-CD SD	0.344 ± 0.002	88.3 ± 1.1	88.4 ± 0.3	86.5

Q_{30} and Q_{60}, drug released at time 30 and 60 min, respectively

DE dissolution efficiency (calculated applying Eq. 5 in an interval of time from 0 to 240 min)

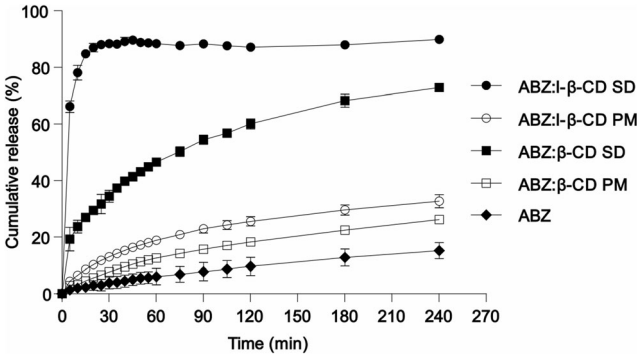

Fig. 9 Dissolution profiles. Release profiles of ABZ (raw material), ABZ loaded in PMs (β-CD and I-β-CD), ABZ loaded in the inclusion complexes prepared by SD (β-CD and I-β-CD). Test conditions 0.1 N HCl, 37 °C ($n = 3$, ± SD)

In vitro evaluation of the anthelmintic activity of the ABZ:I-β-CD systems on *T. spiralis*

The effect of the formulations on the in vitro ability of ABZ to kill adult *T. spiralis* worms was assessed by analysis of the survival curves of the female parasite cultured for 48 h in RPMI 1640 medium containing either I-β-CD, ABZ pure drug or one of the systems (Fig. 10). I-β-CD did not affect the viability of the cultured parasite, the median survival percentage at 48 h being 93.3%. Both the PM and the complex (SD) improved ABZ parasiticidal activity, but only the complex was significantly more active (ABZ vs. complex, $P = 0.0086$). Median survival proportions at 48 h were 88.0% for ABZ, and 72.2% and 55.9% for the PM and the complex, respectively.

The effect of the systems on the NL released by *T. spiralis* females exposed to the antiparasitic solutions was also examined. Control and I-β-CD-treated females showed similar fecundity, as assessed by the number of NL observed in each well, thus suggesting that the modified CD has no antiparasitic activity per se. The number of NL was affected to varying degrees by the antiparasitic treatments. ABZ- and PM-treated females behaved similarly, with an intermediate effect on decreasing fecundity while treatment with the inclusion complex was the most effective.

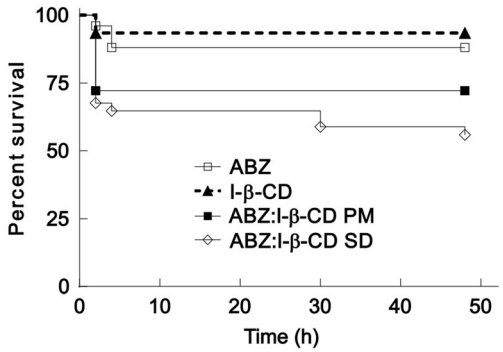

Fig. 10 Analysis of the in vitro parasiticidal effect of the ABZ pure drug and ABZ:I-β-CD systems solutions, on *T. spiralis* adult parasites*. Kaplan-Meier survival curves for female worms cultured for 48 h with the anthelmintic solutions in RPMI 1640 medium; each time point represents the median of three (I-β-CD) measurements. Differences among curves were analyzed with the Mantle-Cox test ($P = 0.0116$). *A description of the procedure is given in M&M.

These results suggest that the ABZ:I-β-CD inclusion complex (SD) would be a promising alternative to produce an efficient antiparasitic pharmaceutical form of ABZ.

Conclusions

The new acidic CD derivative I-β-CD was successfully synthesized. The inclusion complex was prepared and characterized to enhance the solubility of ABZ, a poorly soluble compound with basic characteristics. The charge interaction between I-β-CD and ABZ increased its solubility by complexation. The maximum drug release was reached at 15 min, and the inclusion complex solubility was 88-fold higher than that of the pure drug. Also, the in vitro assay of the system's anthelmintic activity showed that the complex was significantly more effective than pure ABZ. This inclusion complex may prove adequate to be used for oral administration since the physicochemical considerations suggested a significant improvement in the solubility and the dissolution rate of the pure drug.

Acknowledgements J.P. and A.G. are grateful to CONICET (Consejo Nacional de Investigaciones Científicas y Técnicas) for a Doctoral and a Posdoctoral Fellowship.

Funding information This work was supported by the Universidad Nacional de Rosario, CONICET (Project No. PIP 112-201001-00194) and Agencia Nacional de Promoción Científica y Tecnológica (Project No. PICT 2006-1126).

Compliance with ethical standards

Conflict of interest The authors declare that they have no conflict of interest.

Animal studies All institutional and national guidelines for the care and use of laboratory animals were followed.

References

1. Sosnik A, Augustine R. Challenges in oral drug delivery of antiretrovirals and the innovative strategies to overcome them. Adv Drug Deliv Sys. 2016;103:105–20.
2. Sharma P, Garg S. Pure drug and polymer based nanotechnologies for the improved solubility, stability, bioavailability and targeting of anti-HIV drugs. Adv Drug Deliv Sys. 2010;62:491–502.
3. Jambhekar SS, Breen P. Cyclodextrins in pharmaceutical formulations II: solubilization, binding constant, and complexation efficiency. Drug Discov Today. 2016;21:363–8.
4. Kurkov SV, Loftsson T. Cyclodextrins. Int J Pharm. 2013;453:167–80.

5. Frömming K-H, Szejtli J. Cyclodextrins in pharmacy. In: Topics in inclusion complexes. Volume 5, Chapter 1. Springer Science & Business Media; 1993.
6. Schwarz DH, Engelke A, Wenz G. Solubilizing steroidal drugs by β-cyclodextrin derivatives. Int J Pharm. 2017;531:559–67.
7. Jansook P, Ogawa N, Loftsson T. Cyclodextrins: structure, physicochemical properties and pharmaceutical applications. Int J Pharm. 2018;535:272–84.
8. Shelley H, Babu RJ. Role of cyclodextrins in nanoparticle based drug delivery systems. J Pharm Sci. 2018;107:1741–53.
9. García A, Leonardi D, Salazar MO, Lamas MC. Modified β-cyclodextrin inclusion complex to improve the physicochemical properties of Albendazole. Complete in vitro evaluation and characterization. PLoS One. 2014;9:e88234.
10. García A, Leonardi D, Lamas MC. Promising applications in drug delivery systems of a novel β-cyclodextrin derivative obtained by green synthesis. Bioorg Med Chem Lett. 2016;26:602–8.
11. García A, Leonardi D, Vasconi MD, Hinrichsen LI, Lamas MC. Characterization of albendazole-randomly methylated-β-cyclodextrin inclusion complex and in vivo evaluation of its antihelmitic activity in a murine model of Trichinellosis. PLoS One. 2014;9:e113296.
12. Adeoye O, Cabral-Marques H. Cyclodextrin nanosystems in oral drug delivery: a mini review. Int J Pharm. 2017;531:521–31.
13. Codina AV, García A, Leonardi D, Vasconi MD, Di Masso RJ, Lamas MC, et al. Efficacy of albendazole:β-cyclodextrin citrate in the parenteral stage of Trichinella spiralis infection. Int J Biol Macromol. 2015;77:203–6.
14. Priotti J, Codina AV, Leonardi D, Vasconi MD, Hinrichsen LI, Lamas MC. Albendazole microcrystal formulations based on chitosan and cellulose derivatives: physicochemical characterization and in vitro parasiticidal activity in Trichinella spiralis adult worms. AAPS PharmSciTech. 2017;18:947–56.
15. Madsen CM, Feng K-I, Leithead A, Canfield N, Jørgensen SA, Müllertz A, et al. Effect of composition of simulated intestinal media on the solubility of poorly soluble compounds investigated by design of experiments. Eur J Pharm Sci. 2018;111:311–9.
16. Lucio D, Irache JM, Font M, Martínez-Ohárriz MC. Nanoaggregation of inclusion complexes of glibenclamide with cyclodextrins. Int J Pharm. 2017;519:263–71.
17. Shibata M, Nozawa R, Teramoto N, Yosomiya R. Synthesis and properties of etherified pullulans. Eur Polym J. 2002;38:497–501.
18. Higuchi T, Connors KA. Phase solubility techniques. Adv Anal Chem Instrum. 1965;4:95.
19. Garcia-Rodriguez J, Torrado J, Bolas F. Improving bioavailability and anthelmintic activity of albendazole by preparing albendazole-cyclodextrin complexes. Parasite. 2001;8:S188–S90.
20. Castillo J, Palomo-Canales J, Garcia J, Lastres J, Bolas F, Torrado J. Preparation and characterization of albendazole β-cyclodextrin complexes. Drug Dev Ind Pharm. 1999;25:1241–8.
21. Marques HC, Hadgraft J, Kellaway I. Studies of cyclodextrin inclusion complexes. I. The salbutamol-cyclodextrin complex as studied by phase solubility and DSC. Int J Pharm. 1990;63:259–66.
22. Bertacche V, Lorenzi N, Nava D, Pini E, Sinico C. Host–guest interaction study of resveratrol with natural and modified cyclodextrins. J Incl Phenom Macrocycl Chem. 2006;55:279–87.
23. United States Pharmacopoeia Convention. USP 32 NF 27: United States Pharmacopoeia and National Formulary, Volume 1. Rockeville (MD); 2008.
24. García A, Leonardi D, Piccirilli GN, Mamprin ME, Olivieri AC, Lamas MC. SSpray drying formulation of albendazole microspheres by experimental design. In vitro–in vivo studies. Drug Dev Ind Pharm. 2015;41:244–52.
25. Vasconi MDBG, Codina AV, Indelman P, Di Masso RJ, Hinrichsen LI. Phenotypic characterization of the response to infection with trichinella spiralis in genetically defined mouse lines of the CBi-IGE stock. Open J Vet Med. 2015;5:111–22.
26. García A, Barrera MG, Piccirilli G, Vasconi MD, Di Masso RJ, Leonardi D, et al. Novel albendazole formulations given during the intestinal phase of Trichinella spiralis infection reduce effectively parasitic muscle burden in mice. Parasitol Int. 2013;62:568–70.
27. O'Neill M, Mansour A, DiCosty U, Geary J, Dzimianski M, McCall SD, et al. An in vitro/in vivo model to analyze the effects of flubendazole exposure on adult female Brugia malayi. PLoS Negl Trop Dis. 2016;10:e0004698.
28. Pralhad T, Rajendrakumar K. Study of freeze-dried quercetin–cyclodextrin binary systems by DSC, FT-IR, X-ray diffraction and SEM analysis. J Pharm Biomed Anal. 2004;34:333–9.
29. Steiner T, Koellner G. Crystalline. Beta.-cyclodextrin hydrate at various humidities: fast, continuous, and reversible dehydration studied by X-ray diffraction. J Am Chem Soc. 1994;116:5122–8.
30. Mangolim CS, Moriwaki C, Nogueira AC, Sato F, Baesso ML, Neto AM, et al. Curcumin–β-cyclodextrin inclusion complex: stability, solubility, characterisation by FT-IR, FT-Raman, X-ray diffraction and photoacoustic spectroscopy, and food application. Food Chem. 2014;153:361–70.
31. Wei M, Wang J, He J, Evans DG, Duan X. In situ FT-IR, in situ HT-XRD and TPDE study of thermal decomposition of sulfated β-cyclodextrin intercalated in layered double hydroxides. Microporous Mesoporous Mater. 2005;78:53–61.
32. Ficarra R, Tommasini S, Raneri D, Calabro M, Di Bella M, Rustichelli C, et al. Study of flavonoids/β-cyclodextrins inclusion complexes by NMR, FT-IR, DSC, X-ray investigation. J Pharm Biomed Anal. 2002;29:1005–14.
33. Fernandes CM, Carvalho RA, da Costa SP, Veiga FJ. Multimodal molecular encapsulation of nicardipine hydrochloride by β-cyclodextrin, hydroxypropyl-β-cyclodextrin and triacetyl-β-cyclodextrin in solution. Structural studies by 1H NMR and ROESY experiments. Eur J Pharm Sci. 2003;18:285–96.
34. Lezcano M, Al-Soufi W, Novo M, Rodríguez-Núñez E, Tato JV. Complexation of several benzimidazole-type fungicides with α-and β-cyclodextrins. J Agric Food Chem. 2002;50:108–12.
35. Jahed V, Zarrabi A, Bordbar A-K, Hafezi MS. NMR (1H, ROESY) spectroscopic and molecular modelling investigations of supramolecular complex of β-cyclodextrin and curcumin. Food Chem. 2014;165:241–6.
36. Jullian C, Orosteguis T, Pérez-Cruz F, Sánchez P, Mendizabal F, Olea-Azar C. Complexation of morin with three kinds of cyclodextrin: a thermodynamic and reactivity study. Spectrochim Acta A Mol Biomol Spectrosc. 2008;71:269–75.
37. Jullian C, Cifuentes C, Alfaro M, Miranda S, Barriga G, Olea-Azar C. Spectroscopic characterization of the inclusion complexes of luteolin with native and derivatized β-cyclodextrin. Bioorg Med Chem. 2010;18:5025–31.